AIAA Aviation
13-17 June 2016, Washington, D.C.
8th AIAA Flow Control Conference

AIAA 2016-4082

Computational Design of Drag Diminishing Active Flow Control Systems for Heavy Vehicles

David E. Manosalvas*, Thomas D. Economon,†
Stanford University, Stanford, CA, 94305, USA.

Carsten Othmer,‡
Volkswagen Group of America Inc., Belmont, CA 94002, USA.

and Antony Jameson§
Stanford University, Stanford, CA, 94305, USA.

The presented work describes the development of a computationally inexpensive method that has been used for the design and study of Active Flow Control (AFC) systems aimed towards drag reduction for heavy vehicles. The AFC devices chosen are Coanda jets, which have been positioned in all four trailing edges of the fully three-dimensional Ground Transportation System (GTS) model. The jet actuation reduces the wake size and increases the base pressure, reducing the pressure differential on the vehicle and ultimately causing a significant drag reduction. The integrated forces on the vehicle have been computed using Reynolds-Averaged Navier-Stokes (RANS) and the jet configuration changes were quantified using SU2, an open-source Computational Fluid Dynamics (CFD) suite. This study ultimately shows an optimized AFC configuration which reduces drag by 15% and the power used by 12% on a 6.5% scale version of the GTS model.

I. Introduction and Motivation

The commercial trucking industry is a keystone of our economy,[1] as heavy vehicles are used on a daily basis to transport products across the country. These vehicles spend the majority of their life-cycle traveling at highway speeds ($\sim$ 70 mph) where over 65 % of the total energy usage goes towards overcoming aerodynamic drag.[2] According to recent studies,[2] the drag on modern trucks could be reduced as much as 50%, which translates into a fuel consumption decrease of 25%. A 12% reduction in fuel consumption across the national fleet of heavy vehicles would save 3.2 billion gallons of diesel per year and prevent the production of 28 million tons of CO_2 emissions.[3]

The aerodynamics of heavy vehicles are mainly characterized by flow separation and the development of low-pressure turbulent wakes.[4] While great aerodynamic improvements have been made on the tractor with the use of passive techniques, there is still room for improvement on the trailer, which is responsible for 50-60 % of the total drag.[5] The majority of drag generated by the trailer is caused by the development of a low pressure wake, which causes a higher resistance to motion, and can be categorized as viscous pressure drag or base drag.

Aside from basic streamlining, viscous pressure drag can be reduced by the use of Active Flow Control (AFC) techniques.[6] AFC systems reduce the amount of separation behind the vehicle, which increases the pressure inside the wake. The pressure increase in the wake reduces the pressure imbalance between the front and rear of the vehicle and results in a reduction of drag. Wind tunnel experiments using Coanda jets positioned on the trailing end of a trailer have shown that these types of AFC systems are capable

*Ph.D. Candidate, Department of Aeronautics & Astronautics, AIAA Student Member.
†Postdoctoral Scholar, Department of Aeronautics & Astronautics, AIAA Senior Member.
‡Senior Scientist and Project Lead, Electronics Research Laboratory; Stanford University Visiting Scholar, Department of Aeronautics & Astronautics.
§Research Professor, Department of Aeronautics & Astronautics, AIAA Fellow.

of maintaining flow attached and of increasing the wake pressure[6] relative to cases without jets. These experiments have demonstrated not only drag reduction, resulting in a net power savings of more than 15%, but also an improvement in vehicle stability and safety through the use of flow injection to compensate for the effect of side forces.[4]

For the effective design of AFC systems, it is necessary to understand the effects that each part of the system has on the flow features. Due to the complexity of the problem and appearance of separation, Large Eddy Simulation (LES) is believed to be the most reliable method when it comes to the simulation of these flows. Unfortunately, this approach increases the computational requirements significantly, making it prohibitively expensive for use in a design process, given current computational resources. In order to be able to use Computational Fluid Dynamics (CFD) for the design of AFC systems, it is necessary to use a combination of tools that will allow us to simulate the flow around heavy vehicles with an acceptable level of accuracy. In previous studies,[7,8] the combination of Jameson-Schmidt-Turkel (JST)[9] numerical scheme and the Shear-Stress-Transport (SST)[10] turbulence model have been demonstrated as a good compromise between accuracy and computational cost for design purposes.

This article builds upon the previous two-dimensional studies and leverages the knowledge of the flow physics that was gained in order to study the three-dimensional Ground Transportation System (GTS) model. The use of a three-dimensional ground vehicle introduces the stabilizing influence of the ground,[11,12] which combined with the low frequency flow oscillations found by Khalighi *et al.*[13] using Unsteady Reynolds-Averaged Navier-Stokes (URANS), justifies the use of Reynolds-Averaged Navier-Stokes (RANS) for the computation of integrated forces in a similar manner as the work presented by Roy *et al.*[14] and Salari *et al.*.[15] Furthermore, the lowest drag condition for the two-dimensional GTS model, outfitted with Coanda Jets in the back, is achieved when the wake is confined and exhibits a steady behavior.[7,8,16] The introduction of this type of AFC in the GTS model further justifies the use of RANS to investigate the effect that the jet strength has on the aerodynamic drag and power consumption of the vehicle. This article presents a parametric study using jet strength to explore the design space of this AFC drag reduction system and examines the aerodynamic effects caused by the jets when minimizing power consumption.

This paper is laid out as follows: in Section II, a detailed description of the GTS geometry, the jet location and configuration, and the flow conditions are presented. Section III introduces the numerical schemes and turbulence model that have been used, presents the computational grids, and a description of the boundary conditions. Furthermore, this section describes the strategy to model the jet flow injection and the variables used to control it. In addition, it explains the design space exploration strategy and the method used to generate the surrogate models. In Section IV, the drag and wake structure of the baseline GTS model are compared to experimental and computational data. The results from the AFC parametric study are summarized, and the configuration with best performance is used to visualize aerodynamic changes and to explain the increase in performance due to the use of this drag reduction system. Finally, Section V summarizes the results and introduces suggestions for future work.

II. Physical Model and Flow Conditions

For the study of the aerodynamic features that characterize separated flows, and the quantification of the effects that add-on drag reduction devices have on the presence of viscous pressure drag, a streamlined model of a heavy vehicle is sufficient.[5,17] Heavy vehicles have a variety of features that contribute towards flow separation, such as mirrors, antennas, gaps, mud flaps, etc., and to eliminate the effect that these have, the GTS[17] model was used. This geometrical model was developed by a United States Department of Energy consortium to focus on the study of viscous pressure drag. The GTS effectively combines both the tractor and the trailer into a single simplified bluff body that has an elliptical leading shape and ends in a sharp straight cut in the back.[17] For the purpose of this study, a 6.5 % scale GTS, similar to the one used by Englar,[6,18] was selected and can be seen in Figure 1. In addition to the base model in Figure 1, a model that includes Coanda jets in all four edges of the flat back was generated and is shown in Figure 2.

We simulate the flow around the GTS model assuming standard air at sea-level treated as a calorically perfect ideal gas. The velocity was chosen to match the average highway speed, which is 31.3 $\frac{m}{s}$ (70 mph) and translates to Mach number of 0.09195 and Reynolds number, using the GTS model width as the length scale, of $359,900$. This condition allows for the validation of integrated force coefficients using the experimental data reported by Storms *et al.*[19] and Englar,[6] as well as the computational results by Roy *et al.*.[14] Furthermore, the information provided by Englar[6] and Pfeiffer *et al.*[4] concerning AFC for ground vehicles was used to

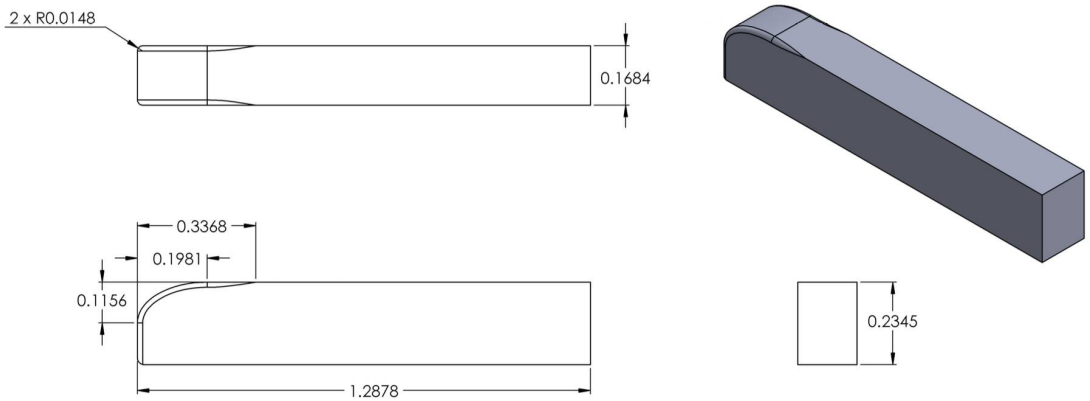

Figure 1: Baseline three-dimensional GTS model - Scale 6.5%. All dimensions in meters.

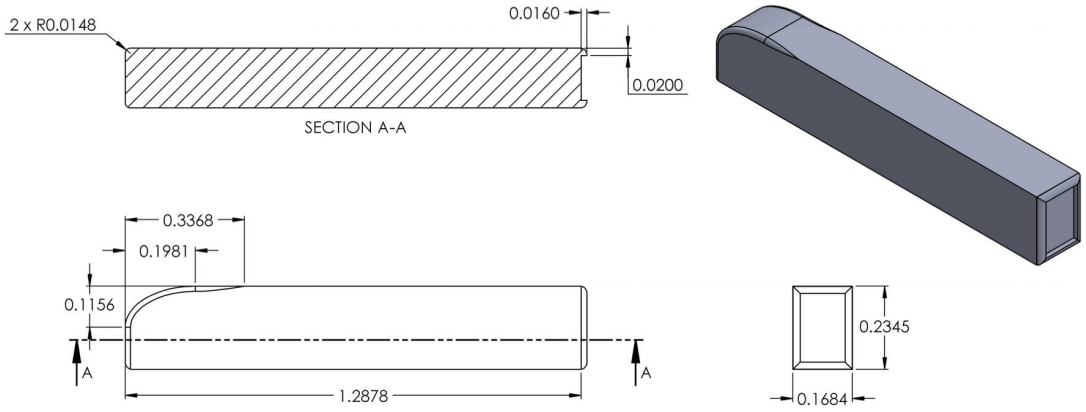

Figure 2: Three-dimensional GTS model with Coanda Jets in the trailing edge - Scale 6.5%. All dimensions in meters.

guide the design space exploration.

The location of all four jets in the back of the GTS was selected to increase reattachment while limiting the interaction between jets. The size and spatial configuration of the jets were chosen based on the two-dimensional studies performed by the authors.[7,8] For this study, spacing between the top of the jet and the roof of the GTS was eliminated, in an attempt to reduce grid complexity, allowing the jet to begin at the edge and have a thickness of $7.7978E-4\ m$ to maintain the Coanda surface geometry in accordance to the two-dimensional studies. The jet position can be seen in Figure 3. This configuration allows for the majority of the incoming flow to take advantage of high momentum air injection, which helps negotiate the sharp corners and reduces separation.

The effect of this GTS system was quantified by looking at the power required to overcome the aerodynamic drag combined with the power to energize the jets. The power used to overcome drag is defined as

$$P_{aero} = D * U_{\infty}, \tag{1}$$

where D is the aerodynamic drag and U_{∞} is the free-stream velocity. In addition, the power required to energize each Coanda jet is quantified by the change in kinetic energy of the injected fluid scaled by an efficiency factor to account for the losses of the system:

$$P_{comp} = \frac{\frac{1}{2} * \dot{m}_e * V_e^2}{\eta}, \tag{2}$$

where the mass flow rate through the jet is $\dot{m}_e$, V_e is the area-averaged jet velocity, and η is the efficiency factor, which was set to be 90% based on compressor isentropic efficiency values. For this study, the jets were modeled by imposing a velocity profile that was extracted from the two-dimensional results in previous work by the authors.[8]

Non-dimensional coefficients for the drag, lateral forces, and lift have been defined as follows:

$$C_D = \frac{D}{q * A}, \qquad C_{LF} = \frac{LF}{q * A}, \qquad C_L = \frac{L}{q * A}, \tag{3}$$

where C_D is the drag coefficient, q is the dynamic pressure calculated as $\frac{1}{2}\rho_{\infty}U_{\infty}^2$, ρ_{∞} is the free-stream density, A is the cross-sectional area calculated as $W * H$, W is the width and H the height of the base GTS model, C_{LF} is the lateral force coefficient, LF is the dimensional lateral force, C_L is the lift coefficient, and L is the dimensional lift force. To characterize the jet strength and power consumption similar definitions are used:

$$C_{\mu} = \frac{\dot{m}_e * V_e}{q * A}, \qquad C_{Pow} = \frac{P_{aero} + P_{comp}}{q * U_{\infty} * A}, \tag{4}$$

where C_{μ} is the momentum coefficient and C_{Pow} is the power coefficient.

III. Numerical Model

The use of CFD for the design of heavy vehicle drag reduction systems requires a balance between accuracy and computational cost, and a compromise was reached by using the second-order accurate JST[9] convective scheme and a corrected average of gradients viscous scheme[20] for the mean flow, in combination with the SST[10] turbulence model. In our previous two-dimensional studies, these tools were applied in a time-accurate setting with URANS to resolve the periodic nature of the flow. The introduction of AFC systems at the trailing end of the two-dimensional GTS model reduced the frequency of vortex shedding. The optimal configuration for these types of systems occurred when the wake was fully enclosed and, for all practical purposes, resulted in a steady flow field around the vehicle.[8] The influence of the AFC system on the flow field can be seen in Figure 4.

The time-averaged C_D obtained using a URANS approach for the model shown in Figure 4b is 0.5988[8] and its RANS counterpart is 0.5984, which is 0.067% lower. This result contributes towards the hypothesis that introducing AFC drag reduction systems in the two-dimensional model stabilizes the wake and transforms it into a problem that can be treated accurately by a steady-state solver.

A significant factor that needs to be addressed when looking into the aerodynamic simulation of ground vehicles is ground effect. Studies by Kim *et al.*[11] and Agarwal[12] show that ground effect has a stabilizing

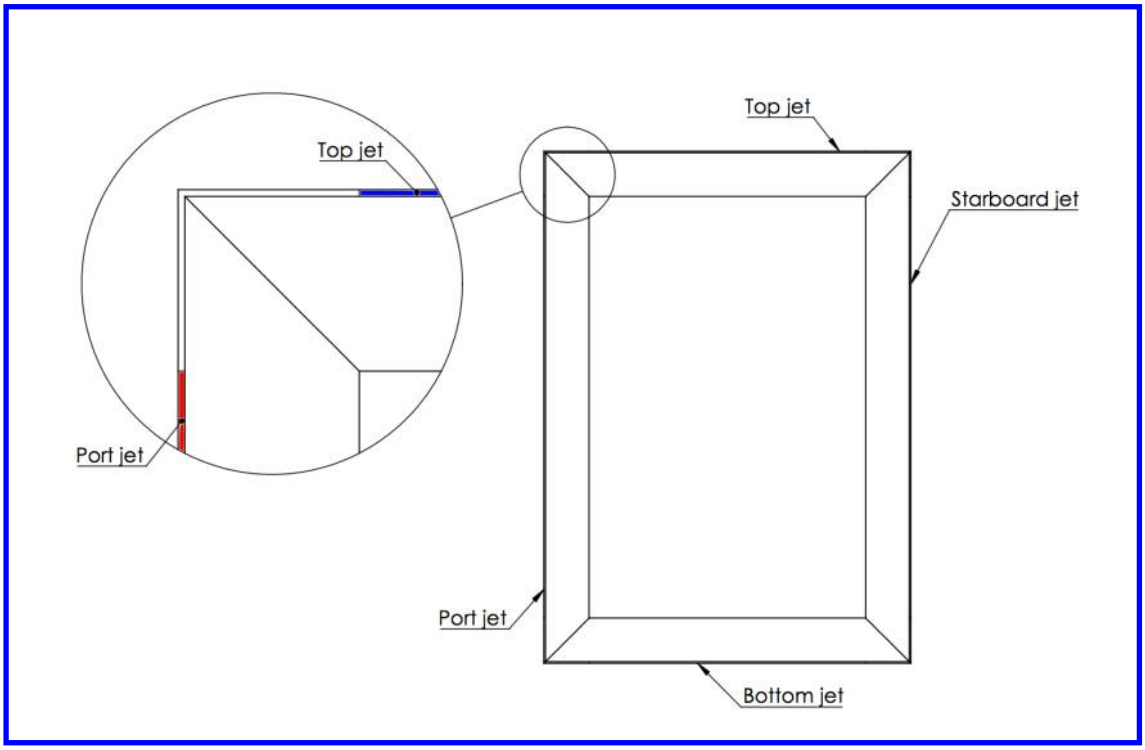

(a) Jet configuration.

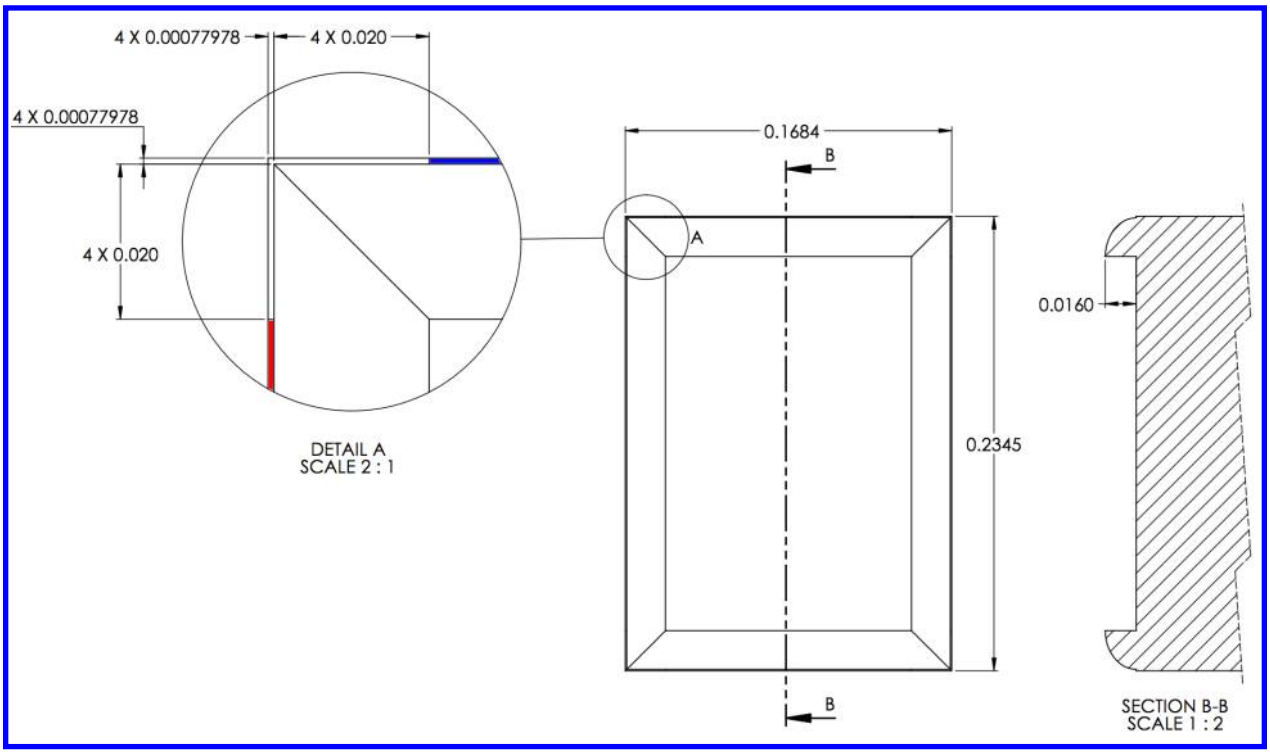

(b) Jet dimensions.

Figure 3: Coanda jets in the back of the enhanced GTS model. In the detailed view the top jet is shown in red and the port jet in blue.

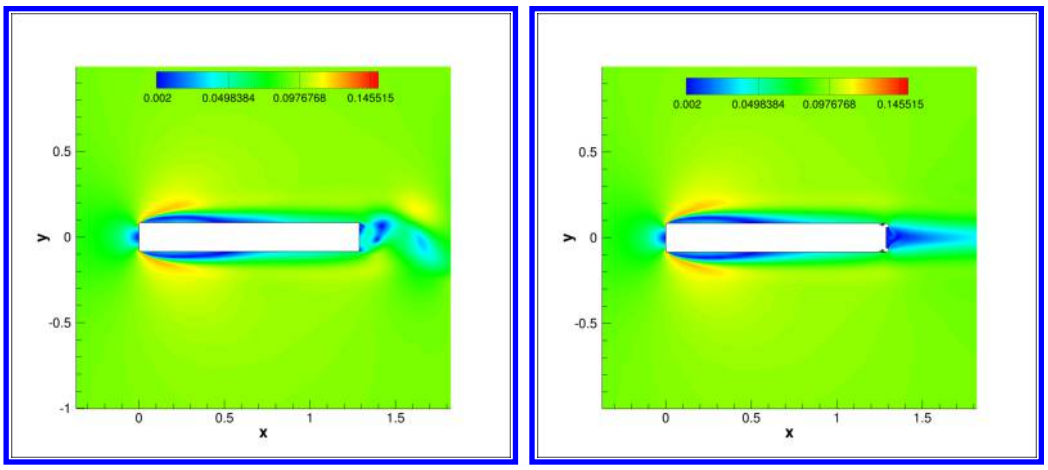

(a) Base GTS model.

(b) Enhanced GTS model with a Coanda radius of 0.0160 m and C_μ of 0.0253.

Figure 4: Mach number contours of the two-dimensional GTS model. Reproduced from Manosalvas *et al.*[8]

influence on the wake with respect to the ground normal component. The added stabilization effect provided by the ground combined with the flow stabilization capabilities of the Coanda jets in the vehicle opens the door for the use of steady-state solvers to design AFC drag reduction systems. Basing our approach on this hypothesis, we perform the design and optimization of this AFC system using the steady-state solver built into the open-source SU2 suite for CFD analysis and design.[21–23]

The computational mesh that was used to represent the GTS geometry is fully unstructured with mixed element types. The boundary layer region is represented by prisms while the rest of the mesh is composed of tetrahedra. The base GTS model mesh has $2,147,204$ points, corresponding to $10,616,539$ cells, and the Coanda jet-equipped GTS has $2,586,690$ points, which corresponds to $11,112,620$ cells. These grids were constructed guaranteeing that the y^+ remains below 1. In the development of these grids, special emphasis was placed on refining the wake region, since this is the area of interest for the design of AFC systems. The base GTS grid can be seen in Figure 5, and the grid for the model with the Coanda jets in Figure 6.

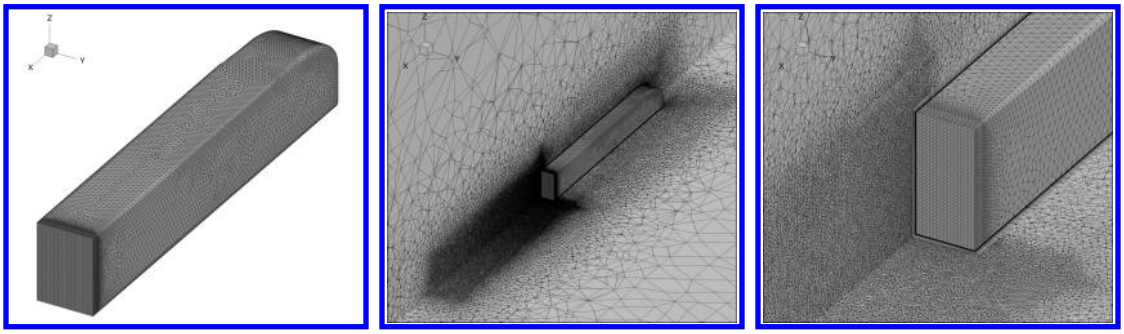

(a) Surface mesh.

(b) Volumetric mesh with planes at y/W = 0 and at z/W = 0.35 .

(c) Back of the GTS with planes in y/W = 0 and z/W = 0.35 .

Figure 5: Grid for the GTS base model.

The GTS surface has been treated using an adiabatic no-slip condition. The far-field boundary of the domain is located in the axial direction at 5 truck lengths from the front and 9 truck lengths from the back. In the direction perpendicular to the flow, the vehicle is centered within 11 truck lengths, and in the direction normal to the ground, the domain spans 5 truck lengths. The outer domain boundaries are treated with the typical characteristic-based far-field condition for external aerodynamics. Finally, the ground plane is modeled using a slip condition, to avoid influencing the solution with the presence of a boundary layer.

To reduce the grid size and the computational resources required for this study, the jets were modeled

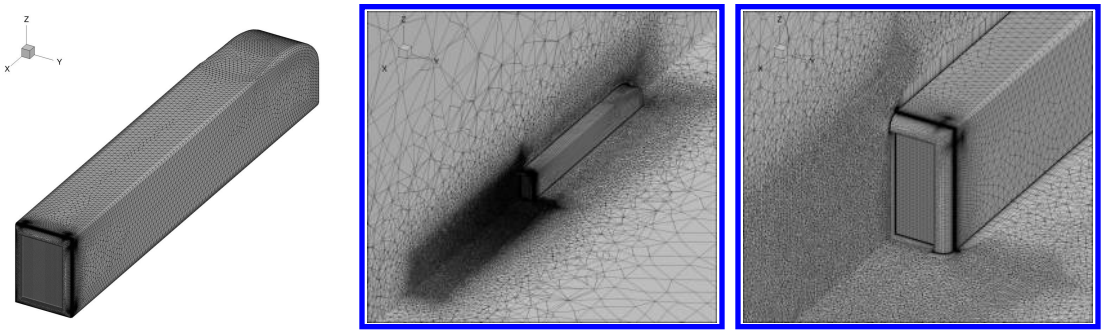

(a) Surface mesh.

(b) Volumetric mesh with planes at y/W = 0 and at z/W = 0.35 .

(c) Back of the GTS with planes in y/W = 0 and z/W = 0.35 .

Figure 6: Grid for the GTS model with Coanda jets .

through boundary conditions with specified velocity profiles, rather than modeling full plenums and nozzles internal to the vehicle. To recover proper behavior, these boundary conditions were implemented in SU2 as characteristic-based inlet conditions[24] with both the velocity and density being specified on the jet face. To model the jets more accurately, velocity profiles were extracted from the two-dimensional optimization published by the authors,[8] and a polynomial was fitted to the data. Once the polynomial was obtained, this was normalized with respect to the peak velocity and, for ease of handling inside SU2, the independent variables were mapped to span from -1 to 1. The velocity polynomial is Equation 5, and the function used to map it is Equation 6.

$$\begin{aligned} P_{bottom}^{top} = -0.7085458261471165\ \tilde{z}^4 \pm 0.0082692314282440\ \tilde{z}^3 \\ -0.2913746290723793\ \tilde{z}^2 \mp 0.008259922266006\ \tilde{z} + 0.9999361038208008, \end{aligned} \tag{5}$$

$$\tilde{z} = \frac{z - z_{min}}{z_{max} - z_{min}} * 2 - 1, \tag{6}$$

where $\tilde{z}$ is the mapped variable that goes from -1 to 1, z is the physical variable, and z_{max} and z_{min} are the physical limits between which the polynomial needs to be mapped. Figure 7 shows the two-dimensional Coanda jet and the normalized extracted polynomial for the top jet mapped to the two-dimensional jet location.

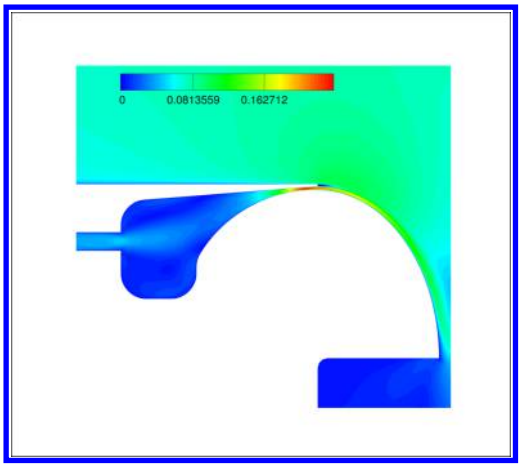

(a) Mach number contour of the two-dimensional top jet. Reproduced from Manosalvas *et al.*[8]

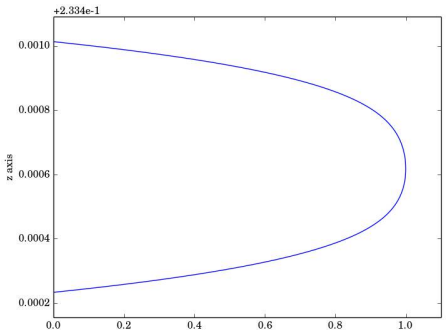

(b) Normalized velocity profile extracted from the top jet.

Figure 7: Velocity profile extracted from the 2D Coanda jet.

The transverse profile of each jet was approximated using a piece-wise function. This approach aims to accommodate the boundary layer growth inside of the plenum. The approximate boundary layer thickness is estimated using the turbulent boundary layer approximation over a flat plate for a flow that has traveled one truck width, or

$$\delta = \frac{0.382\ W}{Re^{1/5}}, \tag{7}$$

$$Re = \frac{\rho_p * V_{peak} * W}{\mu_p}, \tag{8}$$

$$\mu_p = 1.716 * 10^{-5} \left[\frac{T_p}{273.15}\right]^{\frac{3}{2}} \left[\frac{273.15 + 110.4}{T_p + 110.4}\right], \tag{9}$$

where δ is the boundary layer thickness, W is the GTS model width, Re is the Reynolds number, ρ_p is the jet density calculated assuming the injected flow to be an ideal gas at $T_p = 290\ K$ and a pressure of 101325 Pa, V_{peak} is the peak velocity of the jet, and μ_p is the jet viscosity computed using Sutherland's law.[25]

For ease of handling of the function within SU2, it has been normalized with respect to the peak velocity and the independent variable mapped to span between -1 and 1 with the following relations:

$$R = \begin{cases} 1 - \frac{4}{4\tilde{\delta}^2} * (\tilde{y} + 1 - \tilde{\delta})^2 & \text{if } -1 < \tilde{y} < -1 + \tilde{\delta}, \\ 1 & \text{if } -1 + \tilde{\delta} < \tilde{y} < 1 - \tilde{\delta}, \\ 1 - \frac{4}{4\tilde{\delta}^2} * (\tilde{y} - 1 + \tilde{\delta})^2 & \text{if } 1 - \tilde{\delta} < \tilde{y} < 1. \end{cases} \tag{10}$$

This normalized velocity profile mapped to the top jet can be seen in Figure 8a. The velocity profile is handled in the same way for the other jets. The function that represents the full three-dimensional jet velocity profile is shown as $M(z, y)$ in Equation 11, and the three-dimensional profile can be seen in Figure 8b.

$$M(z, y) = P(z) * R(y) * V_{peak} \tag{11}$$

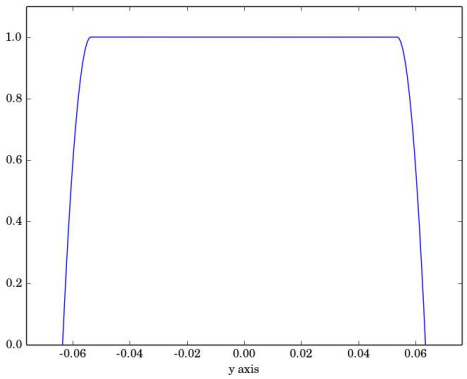

(a) Normalized transverse velocity profile for the top jet.

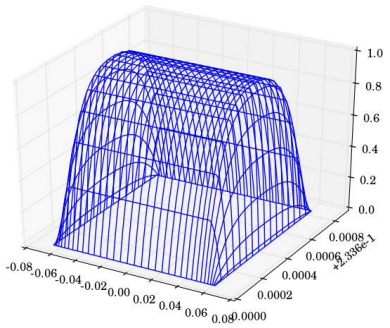

(b) Normalized three-dimensional profile for the top jet.

Figure 8: Jet velocity profile.

A. Design Space Exploration and Parametric Study

To properly design AFC systems capable of significantly reducing harmful emissions and vehicle energy consumption, it is important to understand the effects that jet injection strength has on the overall aerodynamic behavior of the vehicle. As such, we have performed a parametric study that maintains the momentum coefficient (C_μ) constant across all four jets. The drag (C_D) and power (C_{Pow}) coefficients have been computed from the numerical simulation, and a continuous model of their behavior was generated using Gaussian Process Regression (GPR).[26] This approach is used to generate a surrogate model of the system by fitting

a curve in a probabilistic manner through the points evaluated. Additionally, this technique provides an uncertainty metric, represented by a covariance function,[26] which can be used to guide the selection of future function evaluations as well as to have a metric for the uncertainty involved in the surrogate model. In this study, an squared exponential kernel was used for the covariance function, which is a representation of the standard deviation.

The C_μ of all four jets combined was selected to vary between 0.00 and 0.0489, based on the work by Pfeiffer[4] and the experience from previous work on this topic by the authors. C_μ was controlled by varying the peak velocity, which in turn changes the velocity profile. For the present jet configuration, the jet areas for both the top and bottom jets are the same, and the areas for the port and starboard jets are the same, but they differ between them. This disparity causes the peak velocity to be different between the two groups in order to maintain a constant C_μ. Table 1 shows the eleven equally-spaced cases that were used to sample the design space.

$\boldsymbol{Case}$	$\boldsymbol{C_\mu}$	$\boldsymbol{C_{\mu_j}}$	$\boldsymbol{V_{tb_{peak}}}$	$\boldsymbol{V_{ps_{peak}}}$
1	0.0000	0.0000	20.6737	16.6907
2	0.0049	0.0012	29.2089	23.5887
3	0.0098	0.0024	35.7544	28.8796
4	0.0147	0.0037	41.2705	33.3389
5	0.0196	0.0049	46.1291	37.2670
6	0.0245	0.0061	50.5208	40.8178
7	0.0294	0.0073	54.5586	44.0827
8	0.0342	0.0086	58.3165	47.1214
9	0.0391	0.0098	61.8456	49.9751
10	0.0440	0.0110	65.1831	52.6740
11	0.0489	0.0122	42.9844	34.7245

Table 1: Summary of the momentum coefficient and the corresponding velocities for each jet. C_μ is the total momentum coefficient, C_{μ_j} is the momentum coefficient per jet, $V_{tb_{peak}}$ is peak velocity for the top and bottom jets in $\frac{m}{s}$, $V_{ps_{peak}}$ is the peak velocity for the port and starboard jets in $\frac{m}{s}$.

IV. Results

The use of RANS for the simulation of the flow past the basic GTS model has first been compared to experimental results. Since the cylindrical supports that hold the model in place have not been modeled in this computational study, a correction has been used for comparison. To approximate the additional drag caused by having one cylindrical support at the bottom of the GTS model, a two-dimensional diameter-based drag coefficient of 1 was used. The ground clearance of the vehicle was used as the strut length, which is 0.0447 m, the diameter was taken to be 0.05613 m, which is a third of the GTS width, leading to a three-dimensional GTS-area-based drag coefficient of 0.06354, which was added to the vehicle aerodynamic C_D. Table 2 summarizes the results found in the literature as well as the results obtained in the present study.

$\boldsymbol{Contribution}$	$\boldsymbol{Re_W}$	$\boldsymbol{C_D}$
Storms et al., 2001[19]	$360,000$	$0.37 - 0.40$
Englar 2001[6]	$359,900$	0.43
Present	$359,900$	0.3323
Present with supports	$359,900$	0.3959

Table 2: Experimental and computational results for the flow past the base GTS model. Re_W is the width based Reynolds number and C_D is the vehicle drag coefficient.

As can be seen, the C_D obtained is in good agreement with the results reported in the literature, and the

values reported without the strut correction will be used as the base case drag moving forward. In addition to the quantitative results shown in Table 2, the wake structure for the base GTS model has been visualized and compared to the results presented by Roy *et al.*[14] and Storms *et al.*.[19] Figures 9 and 10 have been generated to match the available data and are in good agreement with the RANS results reported in the literature, but as expected, the experimental Particle Image Velocimetry (PIV) results for the wake structure differ. Despite these differences, the wake stabilizing effect of the ground[11,12] allows for the accurate prediction of integrated forces.

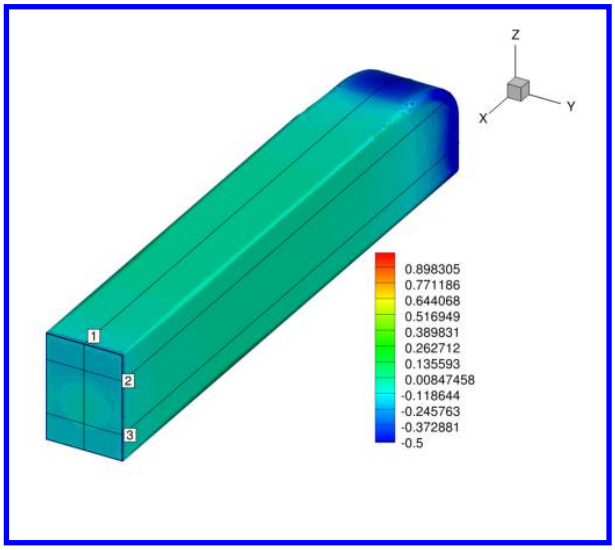

Figure 9: Pressure coefficient and the location of the planes where the wake is visualized in the base GTS model. Cut 1 is located at y/W = 0, cut 2 is located at z/W = 1.05 and cut 3 is located at z/W = 0.35.

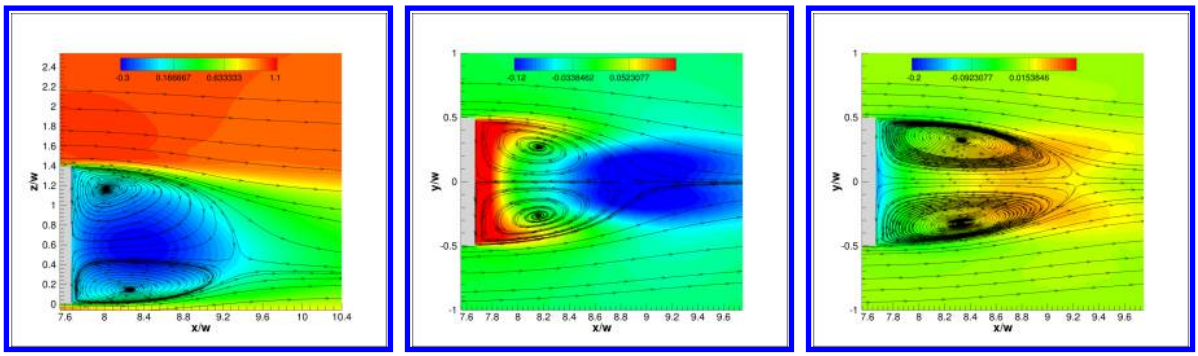

(a) Non-dimensional axial velocity in cut 1.

(b) Non-dimensional velocity normal to the ground in cut 2.

(c) Non-dimensional velocity normal to the ground in cut 3.

Figure 10: Visualization of the wake flow for the base GTS model at a Re_W of 359,900 and a Mach number of 0.09195.

The introduction of Coanda jets along the back of the GTS model stabilizes the wake further, while increasing the back pressure. This AFC system not only reduces drag, but also alters the flow around the vehicle, restraining the wake and increasing its stability. A parametric study was performed by varying the momentum coefficient of the jets to better understand the effect that this AFC system has on the GTS model. Table 3 summarizes the results obtained and Figure 11 shows the response of C_D and C_{Pow} as a function of C_μ.

$Case$	C_μ	C_{μ_j}	C_D	C_{Pow}
1	0.00000	0.00000	0.3154	0.3154
2	0.00489	0.00122	0.3033	0.3045
3	0.00978	0.00245	0.2937	0.2971
4	0.01468	0.00367	0.2869	0.2933
5	0.01957	0.00489	0.2824	0.2921
6	0.02446	0.00612	0.2797	0.2933
7	0.02935	0.00734	0.2783	0.2962
8	0.03425	0.00856	0.2777	0.3003
9	0.03914	0.00978	0.2856	0.3132
10	0.04403	0.01101	0.3118	0.3448
11	0.04892	0.01223	0.3123	0.3509

Table 3: Parametric study results for a Coanda jet-based AFC system mounted in the trailing end of the GTS model. C_μ is the total momentum coefficient, C_{μ_j} is the momentum coefficient per jet, C_D is the drag coefficient and C_{Pow} is the power coefficient.

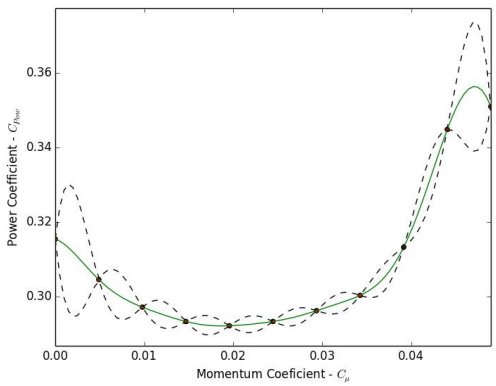

(a) C_{Pow} as function of C_μ. The dashed lines are the bounds for 95% confidence.

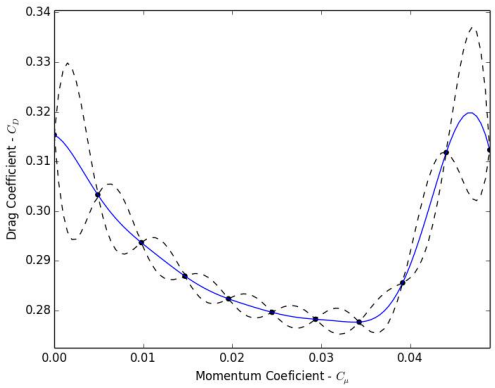

(b) C_D as function of C_μ. The dashed lines are the bounds for 95% confidence.

Figure 11: Surrogate models representing the behavior of power and drag for the GTS model outfitted with Coanda jets.

The surrogate models generated provide a continuous representation of the integrated force and power consumption behavior as the jet strength is varied. This design space representation was used to approximate the jet configuration required to achieve minimum power consumption, which was found at $C_\mu = 0.01869$. The proximity of this configuration to case 5, which is $C_\mu = 0.01957$, and the response surface shape, lead to the selection of case 5 as the minimum power configuration for further investigation. Case 5 generated a $C_D = 0.2824$ and requires a $C_{Pow} = 0.2921$, which is equivalent to a 15% drag and a 12% power reduction with respect to the base GTS model.

The drag and power consumption improvement achieved due to the effect of the AFC system is due to changes in the wake behavior behind the vehicle. As expected, the injection of air through the Coanda jets restrain the wake and reduce it size. Figure 12 shows the wake structure for both the base GTS model and the GTS model with Coanda jets installed.

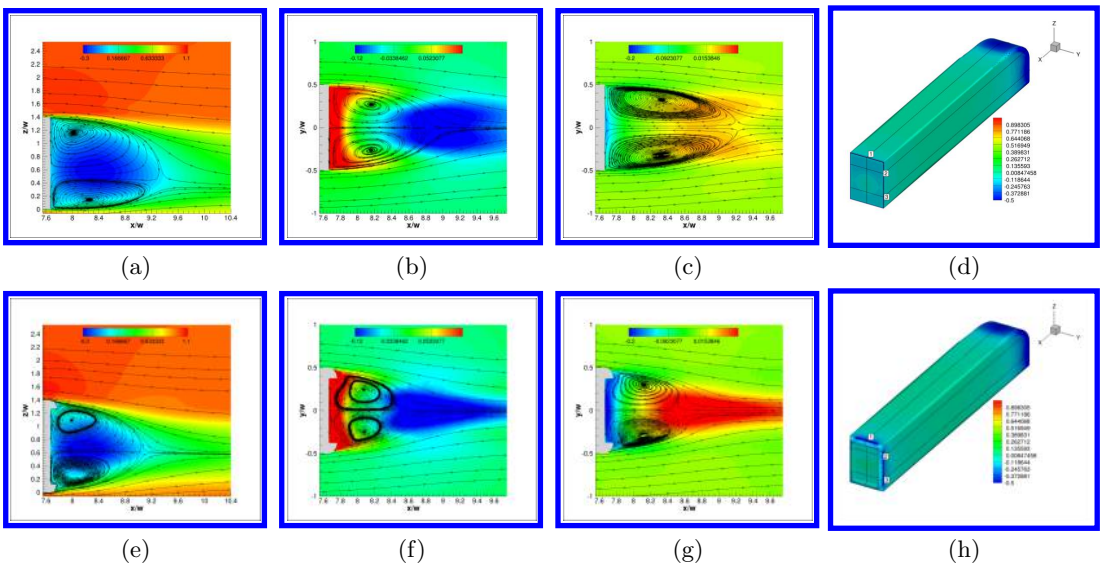

Figure 12: Wake comparison between the base GTS model and the GTS model outfitted with add-on Coanda jets. (a) and (e) show the non-dimensional axial velocity at plane $y/W = 0$, (b) and (f) show the non-dimensional ground normal velocity at plane $z/W = 1.05$, (c) and (g) show the non-dimensional ground normal velocity at plane $z/W = 0.35$, and (d) and (g) the plane locations in the three-dimensional models. Figures (a), (b), (c), and (d) represent the base GTS and figures (e), (f), (g), and (h) the GTS model outfitted with Coanda jets and a total C_μ of 0.01957. Both simulations took place at a width-based Reynolds number of 359,900, and Mach number of 0.09195.

By looking at Figure 12(a) and (e), it can be seen that the wake has not only been reduced in size, but the injection of flow from the bottom jet increases its symmetry and moves the stagnation point further away from the ground. This effect can also be visualized by comparing Figure 12(b) with (f) and (c) with (g), where the magnitude of the ground normal velocity has increased and the distribution shows the symmetry increase. This reduction in wake size leads to an increase in wake stability and symmetry, as well as to a pressure increase on the back of the vehicle. Figure 13 shows the pressure coefficient contours on the GTS vehicle back for both the base and Coanda jet configurations.

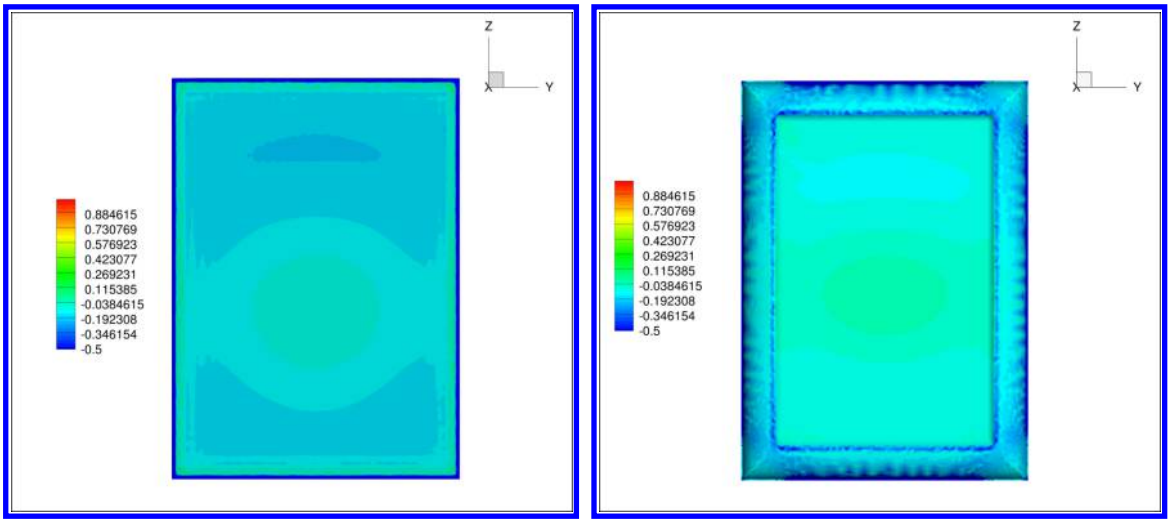

(a) Base case. (b) Enhanced case using a C_μ of 0.01957.

Figure 13: Coefficient of pressure distribution on the back of the base and enhanced GTS model at a Re_W of 359,900 and Mach number of 0.09195.

Comparing Figure 13a and b, we see that the introduction of the Coanda jet AFC system increases the overall pressure on the back face of the vehicle. This view also highlights how the injection of flow through the bottom jet acts to shift the wake core upwards. In addition, it can be seen that the low pressure ring caused by separation on the back of the base GTS vehicle has been eliminated in the regions where the jets are acting, but it has been replaced by localized low pressure regions on the Coanda surfaces. These low pressure regions are caused by the introduction of high speed flow from the jet and are responsible for helping the free stream flow turn around the corner and confine the wake. It is evident that these two effects compete with each other, as the pressure on the flat back surface increases with jet velocity, but the Coanda surface pressure decreases. This effect can be better understood by looking at Figure 14, Figure 11, and Table 4.

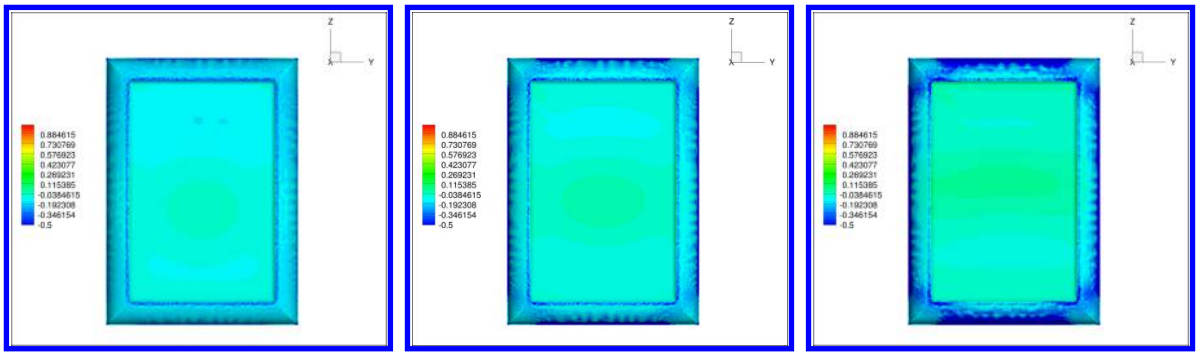

(a) Case 2 where $C_\mu = 0.00489$. (b) Case 5 where $C_\mu = 0.01957$. (c) Case 9 where $C_\mu = 0.03914$.

Figure 14: Coefficient of pressure distribution on the back of the enhanced GTS model at a Re_W of 359,900 and Mach number of 0.09195.

$Case$	C_μ	$C_{D\ back}$	$C_{D\ Coanda}$	C_D	$C_{Pow\ aero}$	$C_{Pow\ comp}$	C_{Pow}
Base	0.00000	0.1810	0.0000	0.3323	0.3323	0.0000	0.3323
2	0.00489	0.0688	0.0714	0.3033	0.3033	0.0012	0.3045
5	0.01957	0.0503	0.0795	0.2824	0.2824	0.0098	0.2921
9	0.03914	0.0300	0.1171	0.2856	0.2856	0.0276	0.3132

Table 4: C_D and C_{Pow} break down. C_μ is the jet momentum coefficient, $C_{D\ back}$ is the drag contribution from the back of the truck, $C_{D\ Coanda}$ is the drag contribution from the Coanda surfaces, C_D is the vehicle drag coefficient, $C_{Pow\ aero}$ is the power required to overcome aerodynamic drag, $C_{Pow\ comp}$ is the power required to energize the jets and C_{Pow} is the overall required power coefficient.

Figure 14a shows a low momentum coefficient configuration where the back pressure increases while the Coanda surface pressure remains relatively high. This allows for a decrease in drag without a significant power consumption increase due to jet actuation. As the momentum coefficient is increased toward its ideal value, the back pressure increases further, and the Coanda surface pressure drops. The pressure contour for this configuration is shown in Figure 14b and the values can be seen in Table 4. The use of this AFC system causes drag reduction, but the rate at which this occurs is reduced due to the competing effect of the integrated forces on these surfaces. In addition, as the momentum coefficient is increased, the power required to actuate the AFC system raises. In case 9, which can be seen in Figure 14c, the momentum coefficient has been increased to a point where the change in drag due to back pressure increase has been completely overshadowed by the pressure decrease on the Coanda surfaces. This configuration not only leads to an increase in the power required to overcome drag, but also to an increase in power required to actuate the jets.

V. Conclusion and Future Work

This article has explored the aerodynamic profile of the GTS model and the use of RANS for the design of Coanda jet-based AFC drag reduction systems. To validate the use of these tools, the integrated forces and wake structure were compared with information available in the literature. To reduce the computational resources required to perform design studies, the authors have implemented a velocity profile inlet in SU2 and used previous two-dimensional aerodynamic studies to inform the jet model for the present three-dimensional investigations.

A parametric study was performed, and surrogate models were used to represent the power and drag behavior as a function of the momentum coefficient for the GTS model outfitted with Coanda jets. The parametric study imposed equal momentum coefficients for all jets. The configuration that uses the minimum amount of power was identified using a GPR driven surrogate model.

The wake structure of the optimized configuration was compared to the base GTS structure, and the mechanisms for achieving drag reduction were identified. Finally, the pressure distribution on the back face of the vehicle for various levels of blowing using the AFC system, as well as the base GTS model were compared. A trade-off exists between the increase in base face pressure and a decrease in Coanda surface pressure, which provides a physical interpretation of the drag and power behavior of the system.

In the future, we aim to understand the aerodynamic changes caused by varying the momentum coefficient of each jet separately. We plan to perform higher fidelity simulations by increasing mesh resolution in the Coanda surface and the wake regions, by using URANS and Detached Eddy Simulation (DES) to find the optimum configuration, and to validate the design by using experimental data. In addition, we would like to investigate the potential to increase the system performance by Coanda surface shape optimization, as well as to explore the use of pulsating and asymmetric jet injection.

VI. Acknowledgments

The authors would like to thank the Stanford Vice Provost for Graduate Education and The Northern California Achievement Rewards for College Scientists (ARCS) fellowship for its support and the Extreme Science and Engineering Discovery Environment (XSEDE)[27] under grant number TG-DMS150004, which is supported by National Science Foundation (NSF) grant number ACI-1053575, for the computational resources required to make this study possible; the members of the Aerospace Computing Laboratory and the Aerospace Design Laboratory at Stanford University for many useful discussions, and the SU2 development team for their hard work maintaining this open source CFD suite.

References

[1] Wood, R., "A Review of Reynolds Number Effects on the Aerodynamics of Commercial Ground Vehicles," *SAE International Journal of Commercial Vehicles*, Vol. 5, No. 2, sep 2012, pp. 628–639.

[2] McCallen, R., Flowers, D., Dunn, T., Owens, J., Browand, F., Hammache, M., Leonard, A., Brady, M., Salari, K., Rutledge, W., Ross, J., Storms, B., Heineck, J., Driver, D., Bell, J., Walker, S., and Zilliac, G., "Aerodynamic Drag of Heavy Vehicles (Class 7-8): Simulation and Benchmarking," *SAE Technical Paper Series*, 2000.

[3] McCallen, R., Salari, K., Ortega, J., DeChant, L., Hassan, B., Roy, C., Pointer, W. D., Browand, F., Hammache, M., Hsu, T., Leonard, A., Rubel, M., Chatelain, P., Englar, R. J., Ross, J., Satran, D., Heineck, J., Walker, S., Yaste, D., and Storms, B., "DOE's Effort to Reduce Truck Aerodynamic Drag - Joint Experiments and Computations Lead to Smart Design," *34th AIAA Fluid Dynamics Conference and Exhibit*, American Institute of Aeronautics and Astronautics, Portland, OR, jun 2004.

[4] Pfeiffer, J. and King, R., "Multivariable Closed-Loop Flow Control of Drag And Yaw Moment For A 3D Bluff Body," *6th AIAA Flow Control Conference*, jun 2012.

[5] van Leeuwen, P. M., *Computational Analysis of Base Drag Reduction Using Active Flow Control*, Ph.D. thesis, Delft University of Tehnology, nov 2009.

[6] Englar, R. J., "Advanced aerodynamic devices to improve the performance, economics, handling, and safety of heavy vehicles," *SAE Technical Paper Series*, 2001.

[7] Manosalvas, D. E., Economon, T. D., Palacios, F., and Jameson, A., "Finding Computationally Inexpensive Methods to Model the Flow Past Heavy Vehicles and the Design of Active Flow Control Systems for Drag Reduction," *32nd AIAA Applied Aerodynamics Conference*, jun 2014.

[8] Manosalvas, D. E., Economon, T. D., Palacios, F., and Jameson, A., "Techniques for the Design of Active Flow Control Systems in Heavy Vehicles," *33rd AIAA Applied Aerodynamics Conference*, American Institute of Aeronautics and Astronautics, Dallas, TX, jun 2015.

[9]Jameson, A., Schmidt, W., and Turkel, E., "Numerical solution of the Euler equations by finite volume methods using Runge Kutta time stepping schemes," *AIAA paper*, jun 1981.

[10]Menter, F. R., "Two-equation eddy-viscosity turbulence models for engineering applications," *AIAA Journal*, Vol. 32, No. 8, aug 1994, pp. 1598–1605.

[11]Kim, T., Lee, B., Lee, D., Lee, D., Hwang, J., and Lee, D., "A Study on Vortex Shedding Around a Bluff Body Near the Ground," *SAE Technical Paper Series*, 2003.

[12]Agarwal, R., "Computational study of drag reduction of models of truck-shaped bodies in ground effect by active Flow control," *SAE Technical Paper Series*, 2013.

[13]Khalighi, B., Zhang, S., Koromilas, C., Balkanyi, S. R., Bernal, L. P., Iaccarino, G., and Moin, P., "Experimental and Computational Study of Unsteady Wake Flow Behind a Bluff Body with a Drag Reduction Device," *SAE Technical Paper Series*, 2001.

[14]Roy, C., Payne, J., and McWherter-Payne, M., "RANS Simulations of a Simplified Tractor/Trailer Geometry," *Journal of Fluids Engineering*, Vol. 128, 2006, pp. 1083.

[15]Salari, K., Ortega, J., and Castellucci, P., "Computational Prediction of Aerodynamic Forces for a Simplified Integrated Tractor-Trailer Geometry," *34th AIAA Fluid Dynamics Conference and Exhibit*, American Institute of Aeronautics and Astronautics, Reston, Virigina, jun 2004.

[16]Englar, R. J., "Improved Pneumatic Aerodynamics for Drag Reduction, Fuel Economy, Safety and Stability Increase for Heavy Vehicles," *SAE Technical Paper Series*, nov 2005.

[17]Gutierrez, W. T., Hassan, B., and Robert, H., "Aerodynamics Overview of the Ground Transportation Systems (GTS) Project for Heavy Vehicle Drag Reduction," *SAE International Congress and Exposition*, 1996.

[18]Englar, R. J., "Development of Pneumatic Aerodynamic Devices to Improve the Performance , Economics , and Safety of Heavy Vehicles," *SEA Technical Paper Series*, 2000.

[19]Storms, B., Ross, J., Heineck, J., Walker, S., Driver, D., and Zilliac, G., "An Experimental System Study of the Ground Transportation System (GTS) in the NASA Ames 7- by 10-Ft Wind Tunnel," *NASA*, feb 2001.

[20]Weiss, J., Maruszewski, J., and Smith, W., "Implicit solution of the Navier-Stokes equations on unstructured meshes," *AIAA paper*, Vol. 2103, 1997, pp. 139–149.

[21]Economon, T. D., Palacios, F., Copeland, S. R., Lukaczyk, T. W., and Alonso, J. J., "SU2: An Open-Source Suite for Multiphysics Simulation and Design," *AIAA Journal*, Vol. 54, No. 3, 2015, pp. 828–846.

[22]Palacios, F., Colonno, M., Aranake, A., Campos, A., Copeland, S., Economon, T. D., Lonkar, A., Lukaczyk, T., Taylor, T., and Alonso, J. J., "Stanford University Unstructured (SU2): An open-source integrated computational environment for multi-physics simulation and design," *51st AIAA Aerospace Sciences Meeting including the New Horizons Forum and Aerospace Exposition*, jan 2013.

[23]Palacios, F., Economon, T. D., Aranake, A., Copeland, S., Lonkar, A., Lukaczyk, T., Manosalvas, D. E., Naik, K., Padron, A. S., Tracey, B., Variyar, A., and Alonso, J. J., "Stanford University Unstructured (SU2): Analysis and Design Technology for Turbulent Flows," *52nd Aerospace Sciences Meeting*, jan 2014.

[24]Hirsch, C., *Numerical Computation of Internal and External Flows*, Wiley, New York, 1984.

[25]Sutherland, W., "The viscosity of gases and molecular force," *Philosophical Magazine Series*, 1893.

[26]Forrester, A., Sobester, A., and Keane, A., *Engineering Design Via Surrogate Modelling: A Practical Guide*, Progress in Astronautics and Aeronautics, Wiley, 2008.

[27]Towns, J., Cockerill, T., Dahan, M., Foster, I., Gaither, K., Grimshaw, A., Hazlewood, V., Lathrop, S., Lifka, D., Peterson, G. D., Roskies, R., Scott, J. R., and Wilkens-Diehr, N., "XSEDE: Accelerating scientific discovery," *Computing in Science and Engineering*, Vol. 16, No. 5, 2014, pp. 62–74.